

# Design Qualification of the Jupiter Icy Moons Explorer JENI Instrument using the LS-DYNA Frequency Domain Suite

M.T. Shanaman<sup>1</sup>, S.A. Cooper<sup>1</sup>, E.A. Rollend<sup>1</sup>, C.E. Schlemm<sup>1</sup>, D.G. Mitchell<sup>1</sup>, P.C. Brandt<sup>1</sup>

<sup>1</sup>The Johns Hopkins University Applied Physics Laboratory, Laurel, Maryland USA

## Summary

In 2022 the European Space Agency (ESA) will launch the JUperiter ICy moons Explorer (JUICE) for an 11-year mission to the Jovian system. The Particle Environment Package (PEP) suite of sensors includes the Jovian Energetic Neutrals and Ions sensor (JENI), designed, built, and qualified by The Johns Hopkins University Applied Physics Laboratory. The requirements established to ensure JENI withstands the launch environment include a first instrument mode above 140 Hz and positive structural margin when subjected to 39g per axis quasi-static analyses and random vibration analyses totaling up to 9.12 g<sub>rms</sub>. To ensure the instrument met these requirements, a detailed LS-DYNA model helped to guide the mechanical design process and ultimately demonstrate the design's suitability for the environment. JENI's small size, coupled with intricate and complex geometries demanded a model with a high element count, 776,868 in all, 52% of which were solid elements. The instrument's design produced a normal modes result with 921 modes between 0 and 2000 Hz, which amounted to a 2.5 hour eigenvalue solution on 20 CPU's. MPP parallelism was especially useful and showed excellent scaling for random vibration analysis in which all output variables for each of the 921 modes over every element needed to be calculated and accumulated for RMS output.

While NASTRAN remains the de facto tool for qualifying space systems throughout ESA and NASA, LS-DYNA's frequency domain suite proved advantageous because its fast run times, robust contact definitions, and MPP solving options. All of the parts in the final design showed a positive stress margin. Simulation responses compared well with experimental results. When ESA required a NASTRAN model for inclusion on the higher-level spacecraft model, a custom Python script performed the conversion from LS-DYNA to NASTRAN. The solutions in LS-DYNA and NASTRAN were found to be in agreement in regard to normal modes and random vibration analysis.

## 1 Model Overview

### 1.1 Instrument Introduction

The Jovian Energetic Neutrals and Ions sensor (JENI) is a NASA-sponsored instrument built by The Johns Hopkins University Applied Physics Laboratory (JHU/APL) as part of the Particle Environment Package (PEP) suite of sensors on ESA's upcoming Jupiter mission, The JUperiter ICy moons Explorer (JUICE). JENI functions as a particle detector, and its mechanical design facilitates this purpose [1]. The most striking feature of JENI is the twin set of AlBeMet deflection blades set up in a pattern to control the flow of particles entering the sensor into a subset of vectors that pass through shutter assemblies and into the main sensor housing, similar to the function of a collimator. Each set of blades is end-supported by a set of Ultem supports mounted to titanium endplates which are in turn connected to a tungsten-copper chassis. Between each blade in the assembly are a set of four Ultem spacers designed to help control blade deflection during vibration. The two deflection blade assemblies are centrally connected to each other by a titanium truss structure (Fig. 1).

The chassis is mounted to the spacecraft via six titanium feet, thermally isolated from the spacecraft by G-10 washers and spacers. The chassis assembly consists of three stacked electronics board assemblies and two sensor assemblies consisting of microchannel plates (MCPs) with supporting electronics and hardware.

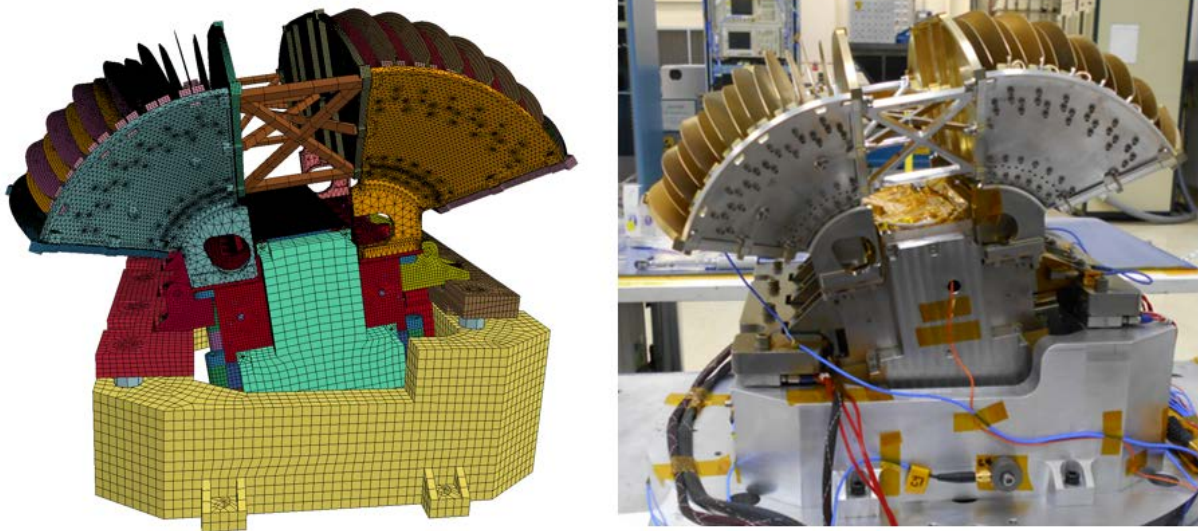


Fig.1: Left: JENI finite element model; Right: JENI Mechanical Test Model prepared for vibration testing

## 1.2 Instrument Structural Requirements

The flight requirements for JENI consist of a first vibration mode above 140 Hz and positive structural margin when subjected to 39g quasi-static design load and random vibration in each of the three spacecraft directions. In-plane and out-of-plane random vibration requirements in the form of acceleration spectral densities (ASDs) in the range of 20 to 2000 Hz are provided by ESA and tailored to the mass of the instrument (Fig. 2). A sine sweep test from 0 to 100 Hz is also required (Fig. 3), but the first mode of JENI is greater than 100 Hz and only occurs in the blades. The first major instrument mode is located at 200 Hz, one octave above the last input frequency to the sine test and satisfying the Octave Rule [2]. The sine test is not explicitly modeled since these vibrations essentially amount to a quasi-static acceleration load, already covered by a 39g simulation.

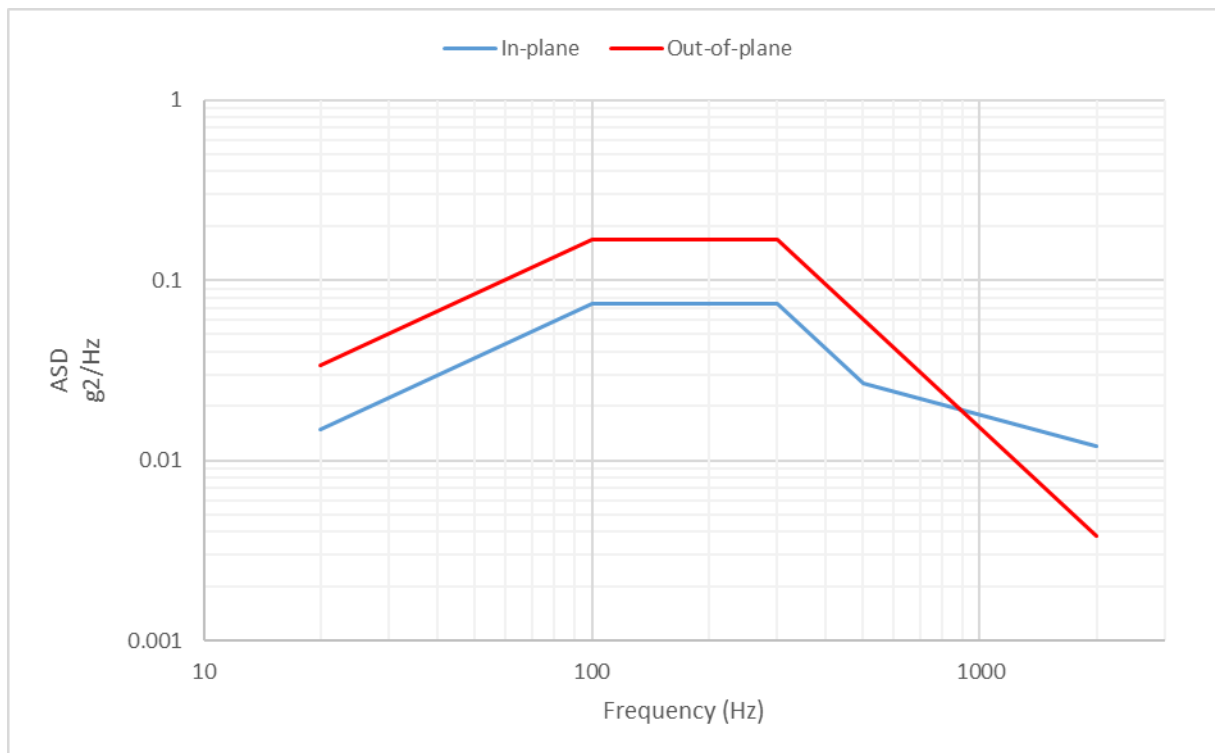


Fig.2: ASD input for random vibration testing for both in-plane (blue) and out-of-plane (red), tailored by ESA to the mass of the instrument.

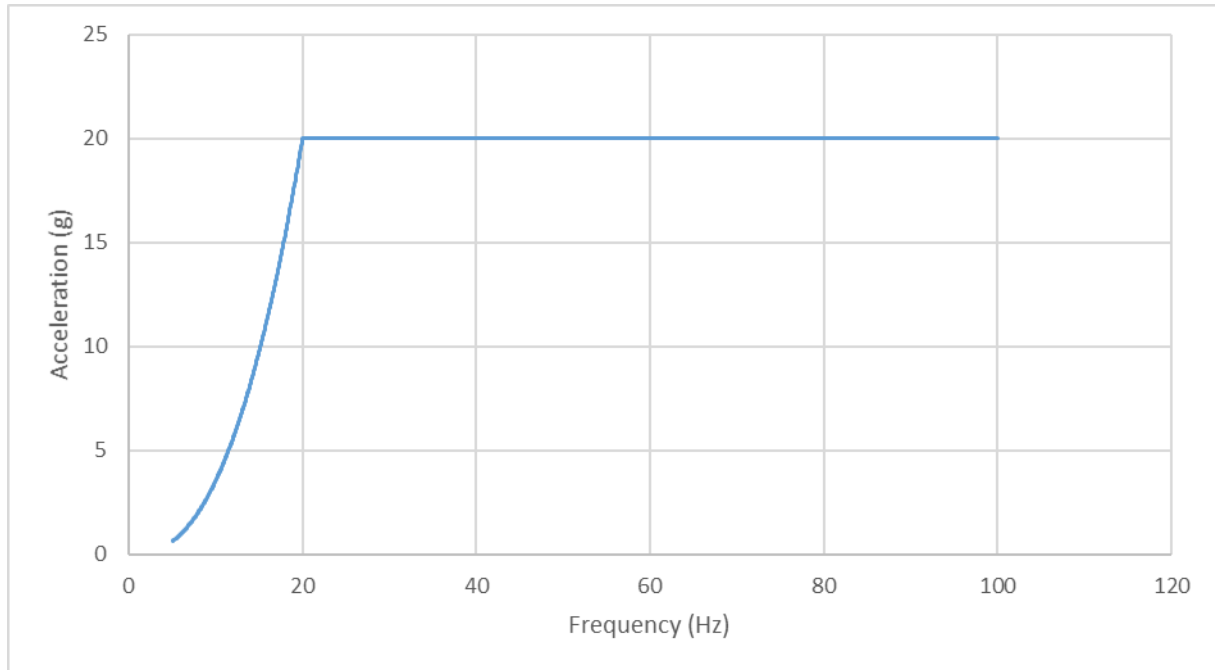


Fig.3: Acceleration input for sine sweep testing, ramping logarithmically to 20g at 20 Hz and ending at 100 Hz. JENI has no modes below 100 Hz so this test essentially behaves as a quasi-static 20g test.

### 1.3 Finite Element Model Construction

The JENI finite element (FE) model was approached as a detailed stress model from the beginning of its construction, aiming to capture the dynamic behavior of an instrument whose size and design does not lend itself to overt simplification. The instrument itself has several parts with complicated geometries that are difficult to approximate with shell elements, and attempts at simplification for FE purposes resulted in eigenvalue solutions that significantly deviated from the behavior of their fully meshed solid counterparts. These complex geometries, including the top housing of the chassis and the four supporting end plates to the deflection assemblies, were meshed with ten-node tetrahedron elements since hexahedron meshing proved unreasonably difficult and time consuming. Most other parts were able to be represented with shell elements and hexahedron solid elements where appropriate. The central truss structure, electronics board stiffeners, and standoffs were represented with beam elements of representative cross sections. Table 1 lists the composition of the FE model and the element formulations used. Masses of all parts were validated to their CAD estimates and adjusted through density definitions or non-structural mass definitions.

	<i>Hex</i>	<i>Tet</i>	<i>Shell</i>	<i>Beam</i>	<i>Mass</i>	<i>Inertia</i>	<i>Nodes</i>
<b>#</b>	222,495	182,579	370,022	1,762	1,850	7	1,071,028
<b>Forms</b>	-2, 3	16	20	13, 2			

Table 1: JENI finite element model composition

The shutter assemblies and the sensor MCPs were simplified to lumped mass representations using **\*ELEMENT\_INERTIA** [3] and inertia tensors derived from CAD. The inertia elements were then tied to their mounting holes via **\*CONSTRAINED\_INTERPOLATION** [3] definitions.

Fastener connections were generally modeled as beam elements connected to mating part holes by **\*CONSTRAINED\_INTERPOLATION** definitions. Originally the model was built with these fasteners as the only means of part connection, knowing that this was likely a “soft” configuration. A counterpart model that introduced contact definitions to most major structural joint interfaces was produced and analyzed alongside the original model prior to experimental testing to ensure that the test results would be enveloped by the two models’ predictions. Experimental results showed that the true behavior did indeed lie between the two models’ predictions, tending closer to those of the contact

model. Contact definitions were adjusted following the tests to tune the final model's response for design qualification.

A finite element model of the testing cradle used in the vibration tests was constructed with hexahedron elements. This model is constrained to "ground" on the bottom surface of the test fixture and the JENI model is attached to it via its interface bolts and the thermal isolators. The G-10 isolators located between the mounting feet and the adaptor as shown in Figure 4 were tested in both solid element and in beam form; no difference was observed between the two representations so the beam format was retained for the qualification efforts. The G-10 washers located on the upper surface of the mounting feet that serve to isolate the bolt head from the mounting feet were modeled explicitly as solid elements.

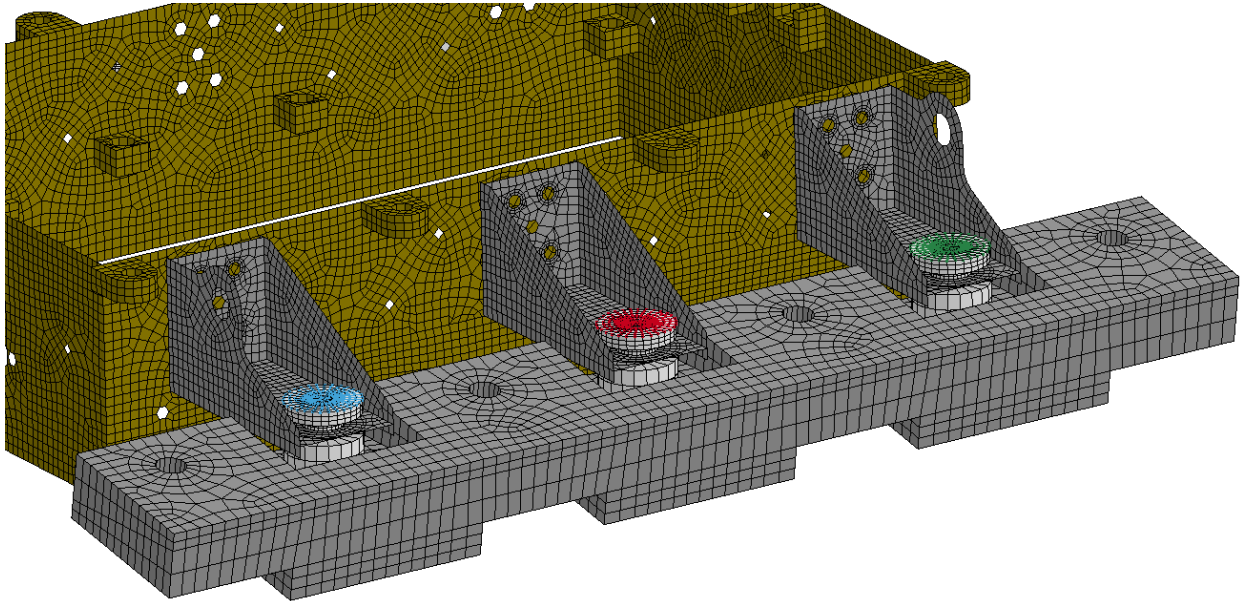


Fig.4: Mounting feet interface to the vibration cradle; G-10 spacers and washers displayed in white

## 2 Model Computational Performance and Behavior

### 2.1 Performance

One of the main motivations to use LS-DYNA as a solver for this model was its demonstrated ability to handle large models, such as those presented by the JENI instrument, in a computationally efficient manner. Not only did JENI require a large model to accurately capture its geometric intricacies, but its design, which includes 26 end-supported thin plates, six electronics boards, and a chassis supported at its midsection by six mounting feet produced a significant amount of complicated natural vibration modes. A typical eigenvalue analysis spanning the frequency range of 0 to 2000 Hz produced on the order of 1000 normal modes, which, for a model this large, takes approximately two and a half hours to solve on one 20-CPU node in a JHU/APL computing cluster using the MPP solver in double precision. Reduction in the frequency range during model iteration and tuning reduced this time to 20 minutes, making for a very efficient tuning procedure.

The random vibration solver benefits greatly from the MPP solving options and shows excellent scaling capability [4]. On 100 CPUs over five nodes, a random vibration analysis of the full 0-2000 Hz spectrum completes in only one hour and eleven minutes. If only operating sequentially, this put the total solve time for a single new model at less than a single work day. Using other automated tools, a full stress margin report is able to be generated in a single work day for every part in the FE model.

### 2.2 Model Characteristics

Due primarily to the nature of the deflection blade assembly consisting of multiple suspended thin plates, the normal modes analysis generates 921 modes between 0 and 2000 Hz. Of these modes,

only 12 have effective mass fractions at the instrument level above 5%, and only 7 of those 12 are above 10%. Many of the modes, including the first mode, consist only of deflection plate movement, and many of those are phased duplicates of each other. Presented in Table 2 are the twelve modes with significant mass contribution and also the first mode, which is a plate-only mode as described previously. Figure 5 visualizes the displacements for the first mode in the plates, the first 3 significant modes in each translational direction, and the largest Z-direction mode which includes significant out-of-plane electronics board movement.

Mode	Frequency (Hz)	Mass Fraction X	Mass Fraction Y	Mass Fraction Z
1	118	0.00%	0.23%	0.00%
27	200	20.75%	0.00%	0.00%
55	257	0.00%	0.08%	6.53%
57	268	0.04%	7.21%	7.47%
58	271	0.00%	29.35%	0.45%
59	275	55.62%	0.00%	0.00%
85	297	0.15%	0.08%	6.49%
86	319	0.08%	1.58%	25.03%
87	326	7.62%	0.30%	6.08%
88	328	0.19%	0.68%	12.83%
103	373	0.00%	1.53%	12.61%
119	401	0.00%	6.61%	0.23%
152	462	0.08%	13.47%	0.71%

Table 2: Table of significant JENI modes and effective modal mass contributions in each translational direction; mass contribution greater than 5% is highlighted

It should be noted that even though the first measured mode is below the 140 Hz threshold, its effective modal mass contribution is extremely small and would not be noticeable to the spacecraft. During experimental testing, the top housing accelerometer, a measurement point analogous to the center of gravity of the instrument, did not measure a noticeable natural frequency until 196 Hz.

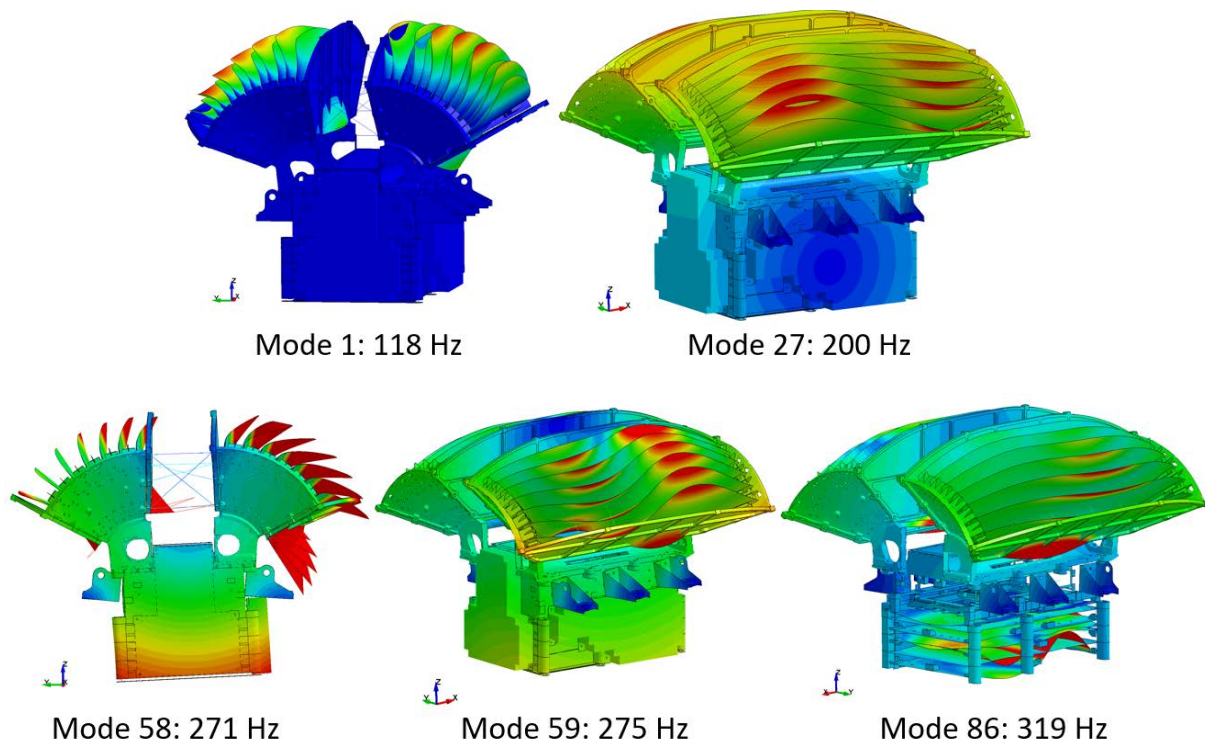


Fig.5: Displacement visualization of the first mode and fundamental modes of JENI

While there are many modes measured in this instrument that are considered insignificant from a modal mass perspective, their summed contribution to random vibration response is quite significant since they represent much of the movement of the blades themselves. In an attempt at increasing solver efficiency a list of extremely low effective mass modes was accumulated and fed into the **\*FREQUENCY\_DOMAIN\_MODE\_EXCLUDE** [3] keyword to exclude the contribution of these modes and therefore reduce the modal superposition computation time. While solve time was definitely reduced by a large factor, this solution deviated significantly from the control solution using all modes, and therefore the exclusion method was not used.

### 3 Experimental Testing

#### 3.1 Procedure

A mechanical test model of JENI was built for testing and subjected to a suite of vibration tests. Each axis was tested independently, and all tests were completed on one axis before adjusting the test fixture and moving on to the next direction. For each axis the same general procedure was followed for the vibration testing:

1. 0.1g sine survey test; 4 octaves/minute sweep rate between 5 and 2000 Hz
2. Sine test between 0 and 100 Hz at 4 octaves/minute sweep rate
3. 0.1g sine survey test; 4 octaves/minute sweep rate between 5 and 2000 Hz
4. Random vibration test
  - a. Short -12dB level check to establish trends and check notch levels
  - b. Progressive 3 dB level increases with 15 second holds
  - c. Full qualification level for 1 minute
5. 0.1g sine survey test; 4 octaves/minute sweep rate between 5 and 2000 Hz

The random vibration test was initiated at levels 12 dB below the qualification specification and increased in 3 dB steps until the full qualification levels are reached. Force limiting was applied to the system per the NASA Technical Handbook NASA-HDBK-7004C [5]. Force limited vibration testing is intended to account for the impedance differences between the actual mounting configuration on the spacecraft and the relatively rigid mounting surface employed for vibration testing. Force limiting provides the system with a means to notch the acceleration input via a feedback loop with force sensors located beneath the mounting feet of JENI. The force limit envelope is created based upon the input ASD curve, the instrument mass, and the fundamental frequency of the system, as directed by the Semi-empirical Method in the NASA handbook.

The low-level sine surveys precede and follow each qualification test not only for the purpose of identifying natural frequencies but also to identify any odd behaviour or changes that may have occurred during a test. The sine surveys are reviewed between each test along with a visual inspection of the instrument in order to identify any changes or breakage that could have occurred during a test.

#### 3.2 Results

The nominal JENI design was tested through the full vibration procedure without breakage or incident. As predicted by the FE models, the sine sweep test functioned as a rigid-body acceleration test as no natural modes were located below 100 Hz.

As an explorative procedure to improve field-of-view for the instrument, JENI was also tested with blade spacers removed in two configurations: removal of the two center-most spacers, and complete removal of the spacers. The configuration with partial removal of spacers performed without issue in the Y-direction, in-plane suite of vibration tests. Before the test configuration was changed, the spacers were completely removed and the instrument again subjected to the Y-direction vibration tests. In this configuration the sine sweep test produced a breakage of some AIBeMet blades and the experiment was terminated.

Materials inspection of fracture sites on the blades suggested that the failures appeared to be ductile fractures that, while progressive and likely growing over multiple oscillations in the sine test, were not indicative of fatigue failure. A finite element model tuned to the results of the nominal test was modified to remove the Ultem spacers in order to examine the stress patterns in the broken blades.

Significantly lowered deflection blade natural frequencies within the sine test range and stress concentrations at the locations identified as the fracture initiation sites support the theory that the breakages were due to excess load and not fatigue-related.

#### 4 Comparison to Experiment and Response Tuning

Prior to the experiment, FEA results were prepared for versions of JENI with and without contact interfaces at the major joint locations. As might be expected, the test results trended toward a solution that seemed to lie between the version with complete contact interfaces and the version without any contact interfaces, tending much more toward the contact-enabled model. The first set of vibration tests in the Z-direction exhibited a fundamental mode measured 18% lower than the contact model; in fact, this 18% to 20% downward shift in natural frequencies from the computational model tended to hold true for subsequent major modes and also in the X and Y directions, allowing the model results to still be used as a general predictive tool during the test procedure.

Following the tests, the next step was to use the results to tune the FE model to be used as an accurate predictive tool for experimentally unmeasured or unmeasurable results such as stress, acceleration, and displacement in many of the structural or sensitive parts of the assembly. For the purpose of tuning the model, multiple tools from the `*FREQUENCY_DOMAIN` [3] suite of functions were used including the Frequency Response Function (FRF) solver (`*FREQUENCY_DOMAIN_FRF` [3]) and the Random Vibration solver (`*FREQUENCY_DOMAIN_RANDOM_VIBRATION` [3]). While LS-DYNA may be known for its legacy explicit dynamics solver, the eigenvalue solver has been implemented and improved upon for roughly twenty years with the intent to keep models compatible with legacy LS-DYNA models and scalable using MPP options [3]. For roughly ten years the frequency domain suite has been implemented to provide robust frequency domain solutions for LS-DYNA models, with steady development adding and validating the functions described above [4] [6] [7].

##### 4.1 Modal Tuning Using Sine Survey Data and FRF Calculations

In frequency domain modeling, all calculations hinge on the eigenvalue analysis as a prerequisite to further frequency analytics [3] [4]. Fortunately, all of the FEM frequency domain keywords in LS-DYNA include the option to restart the analysis based upon a previously run eigenvalue analysis, optionally using the keyword `*FREQUENCY_DOMAIN_PATH` [3] to point to an eigenvalue analysis in another directory. For the purposes of model tuning, frequency extraction was limited to the range between 90 and 600 Hz, keeping each iterative model adjustment's eigenvalue solve time to roughly twenty minutes using MPP on twenty processors.

The experimental sine survey tests were used as the basis for natural frequency identification experimentally, and frequency values at peaks in the top housing accelerometer data were compared to significant model modes as a rough basis for model correlation during coarse adjustments. A finer look at the comparison between model response and sine survey accelerometer data made use of the FRF solver. In essence, the FRF solver provides the response of a selected output variable, such as acceleration, to a unit base input at a single frequency [7]. Provided a list or a range of sampling frequencies, the solver uses the previously conducted eigenvalue solution and modal superposition to provide the total response of nodes identified by the user. By choosing an accelerative input of 1g and selecting a node at the same position as the experimentally placed top housing accelerometer (Fig. 6), the acceleration frequency response function can be scaled by 0.1 to approximate the experimental 0.1g sine sweep. It is worth noting that this scaled FRF solution is not a perfect representation of the sine survey experiment; while the experiment slowly and continuously increases its frequency over time, the FRF solution is an amalgamation of single acceleration data points taken at discrete frequencies. However, under the assumption that the sine sweep was sufficiently slow enough in its progression to differentiate adjacent modes, the comparison of the FRF to the test data can still provide the user with an effective tool for aligning the natural frequencies of the model with the experimental results.

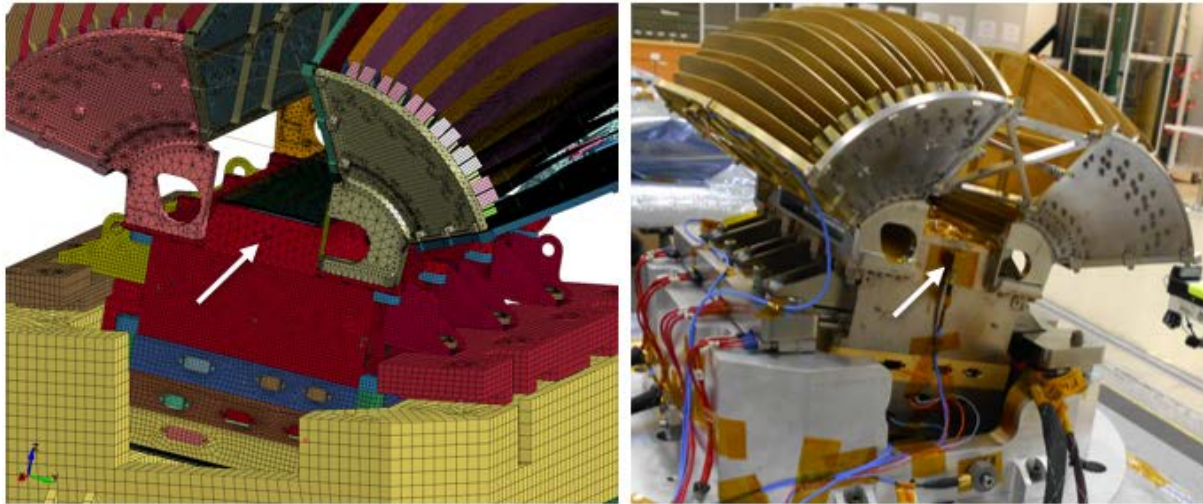


*Fig.6: Right: Top housing accelerometer; Left: Representative node for FRF extraction and comparison to top housing accelerometer data*

Using this comparison method, iterative changes were made to the model to track down stiffness in the system causing the high prediction values. Material stiffnesses of the chassis and the mounting feet were lowered to minimum levels for tungsten-copper and titanium respectively, but these adjustments did not produce the desired magnitude of system stiffness reduction. Next, contact definitions were systematically added or removed to determine their effect on the system.

Contact definition in the frequency domain must be added judiciously. Differing from the typical implementation of contacts for time-domain simulations in LS-DYNA, eigenvalue and frequency domain simulations have no intrinsic mechanism to differentiate between the compressive load of a typical non-sticking contact and the surface separation that would occur upon the reversal or release of that load. Instead, all contacts behave as tied contacts in the normal direction [8] and could run the possibility of overly constraining surface interfaces. It is therefore important to inspect each contact interface for physical behavior and to compare the behavior to experimental results when available. Most contact definitions in the JENI model were found to be required to produce experimentally observed major modes. Extra contact definitions were actually added to internal assemblies in order to keep higher frequencies in closer alignment with experimental data.

The key adjustment to the model that aligned the first major modes turned out to be the removal of the contact definition between the mounting feet and the main chassis body, allowing the beam element screw representations to define what turned out to be the most realistic representation of the joint stiffnesses between the feet and chassis. This was somewhat surprising since this interface is secured by four fasteners, but it was shown that the addition of this contact tended to make the entire system behave in an overly stiff manner.

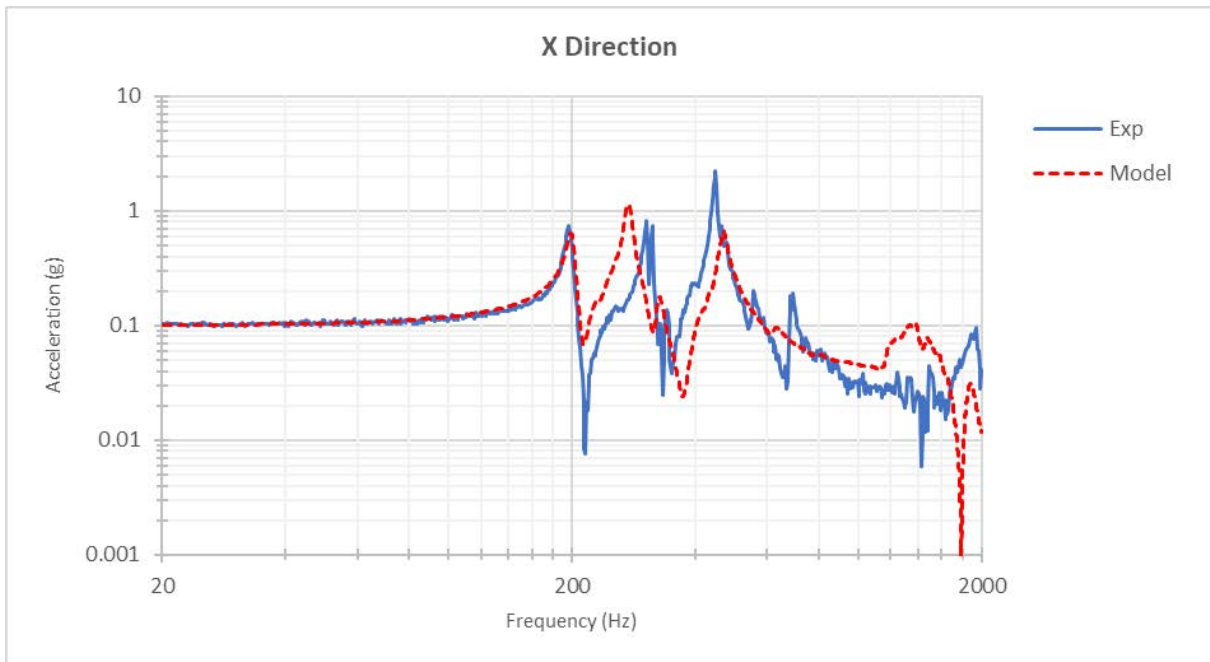


Fig.7: X-direction FRF model comparison to the experimental sine survey test measurements at top housing accelerometer

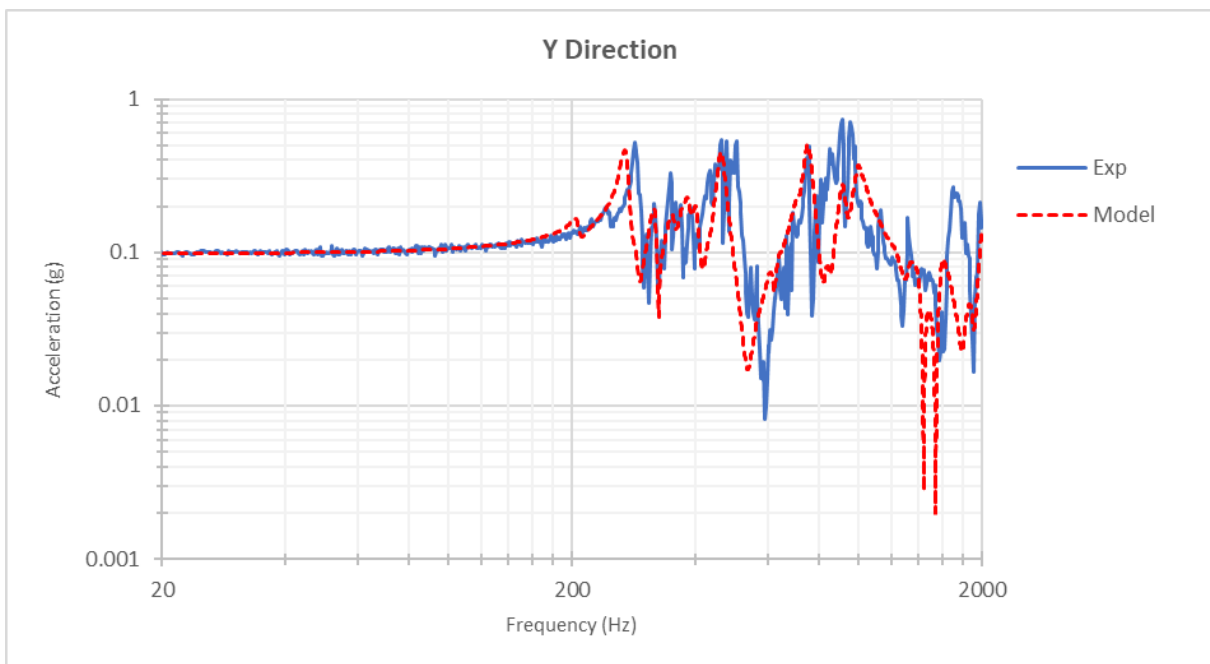


Fig.8: Y-direction FRF model comparison to the experimental sine survey test measurements at top housing accelerometer

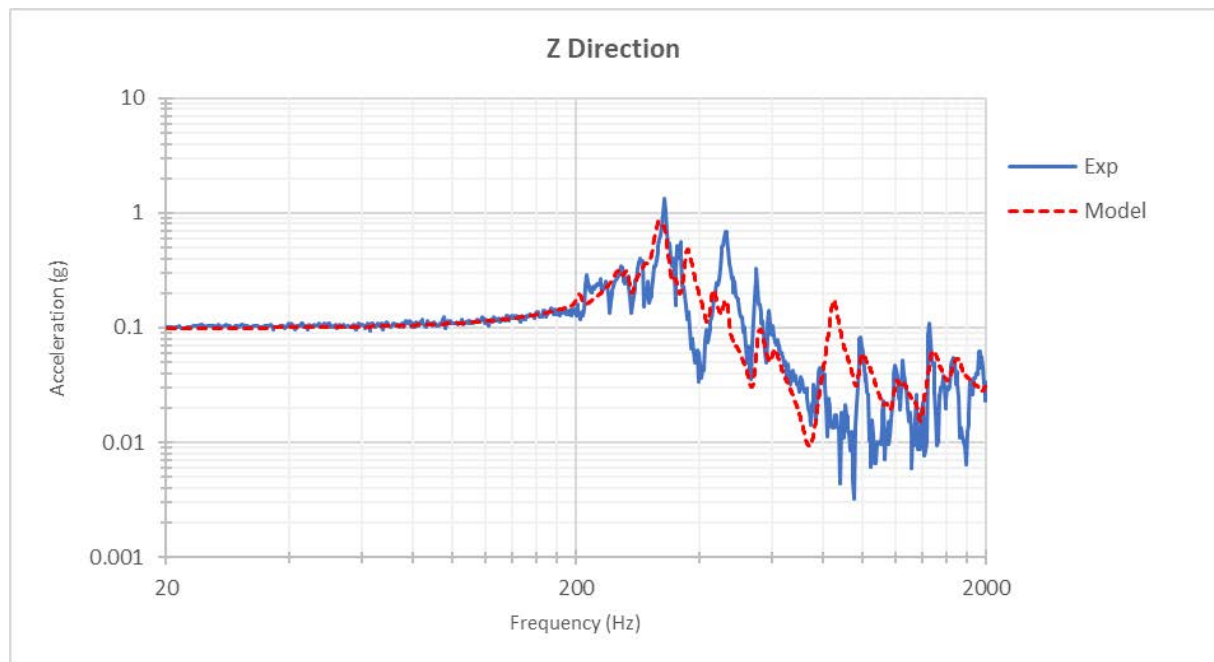


Fig.9: Z-direction FRF model comparison to the experimental sine sweep test measurements at top housing accelerometer

#### 4.2 Validation with Random Vibration

With the modes initially tuned using sine sweep data and FRF calculations, the model ultimately needed to be validated using random vibration. The test input ASDs were extracted and enveloped according to NASA guidelines [9] to include the notches created during the test by the force limiting feedback. This ASD was then fed into the `*FREQUENCY_DOMAIN_RANDOM_VIBRATION` keyword via a curve definition. Each vibration direction received its own unique ASD curve generated from the test data.

The output received from the random vibration solver comes in the form of power spectral density (PSD) and root mean square (RMS) output, controlled by the keywords `*DATABASE_FREQUENCY_BINARY_PSD` [3] and `*DATABASE_FREQUENCY_BINARY_RMS` [3]. The user may specify the PSD sampling points in a number of automatically generated ways, but the size of the JENI model and the large number of normal modes encourages the user use the manual method and to be judicious in choosing the sampling points in order to keep runtimes reasonable. A MATLAB script was written to read the eigenvalue summary (eigout) file generated during the eigenvalue analysis in order to parse modes deemed significant by examining effective modal mass contributions. In order to ensure that blade modes were adequately sampled, a cutoff point of 0.5% effective mass contribution was set in the code. A list of significant modes is generated and augmented in several ways:

1. Starting and ending points are added at 20Hz and 2000Hz, along with points added at 40, 60, and 80Hz for plot smoothness
2. Points are added at frequencies 90%, 95%, 105%, and 110% of each significant mode in order to accurately describe curve peaks
3. Extra points are added to ensure at least one point in a 50Hz span

This method generates a list of PSD sampling points clustered about the major natural frequencies of the model and also maintains a smooth output PSD curve. The RMS output is generated from the PSD sampling points, so it is imperative to select a sufficient number of well-placed points to get accurate RMS data.

Overlaying the top housing accelerometer ASD and the ASD generated at a representative node on the model, a good correlation between model and experiment is observed in regard to natural frequency location (Figs. 10-12) ASD amplitude is most significantly controlled by the critical damping

ratio, designated as DAMPF in the `*FREQUENCY_DOMAIN_RANDOM_VIBRATION` keyword. In general, damping is mode-dependent and may even be input that way by specifying a damping curve ID in the LCDAM parameter; however, the process of creating a modal damping curve is arduous, especially for a model with this amount of normal modes. Damping ranged between 1.3% and 3.5% in most structural modes according to the sine survey data. Damping was also observed to increase along with increased vibration input amplitude, so a conservative value of 1.5% critical damping was chosen as the conservative baseline modal damping coefficient applied across the entire frequency spectrum. Most discrepancies between the model and experiment can be attributed to the lack of frequency-dependent damping; niche applications of the model, such as electronics board analysis were tuned for frequency-dependent damping (Fig. 13) to achieve significantly more accurate results.

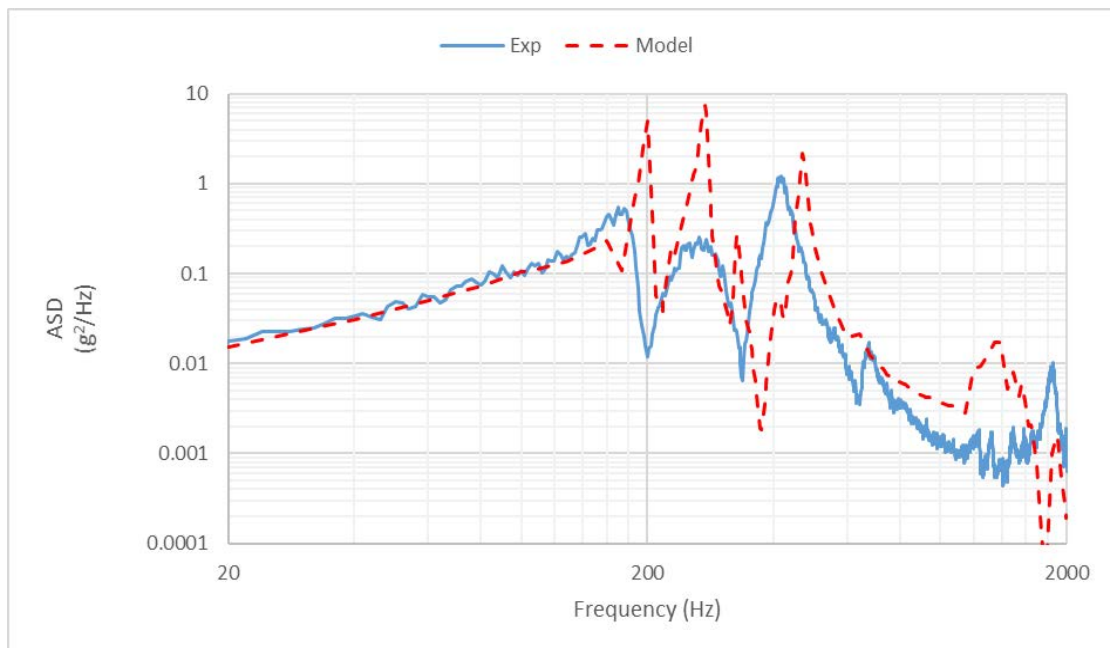


Fig.10: X-direction ASD model comparison to random vibration test at top housing accelerometer; experimental data in solid blue; model data in dashed red.

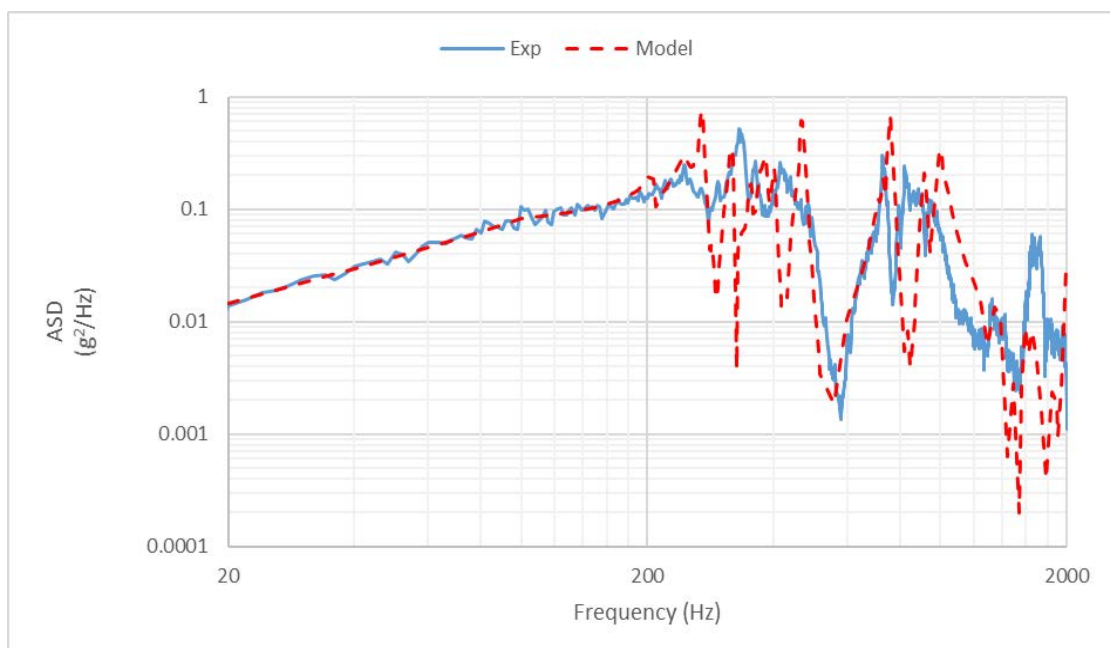


Fig.11: Y-direction ASD model comparison to random vibration test at top housing accelerometer; experimental data in solid blue; model data in dashed red.

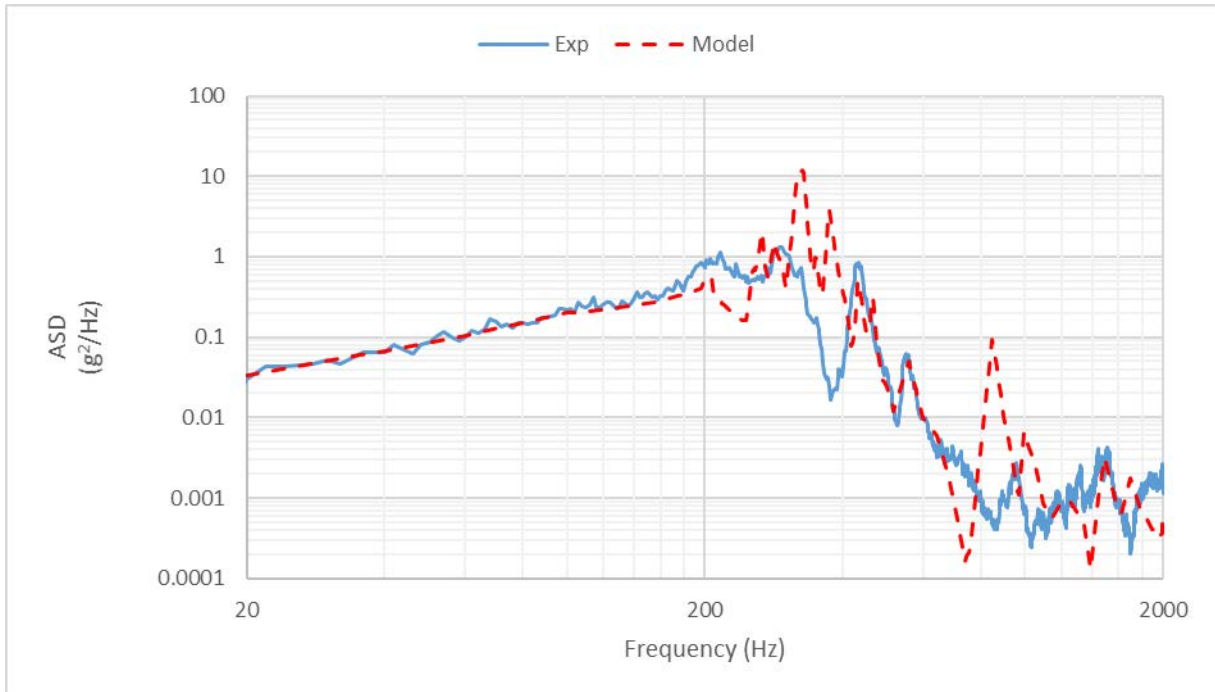


Fig.12: Z-direction ASD model comparison to random vibration test at top housing accelerometer; experimental data in solid blue; model data in dashed red.

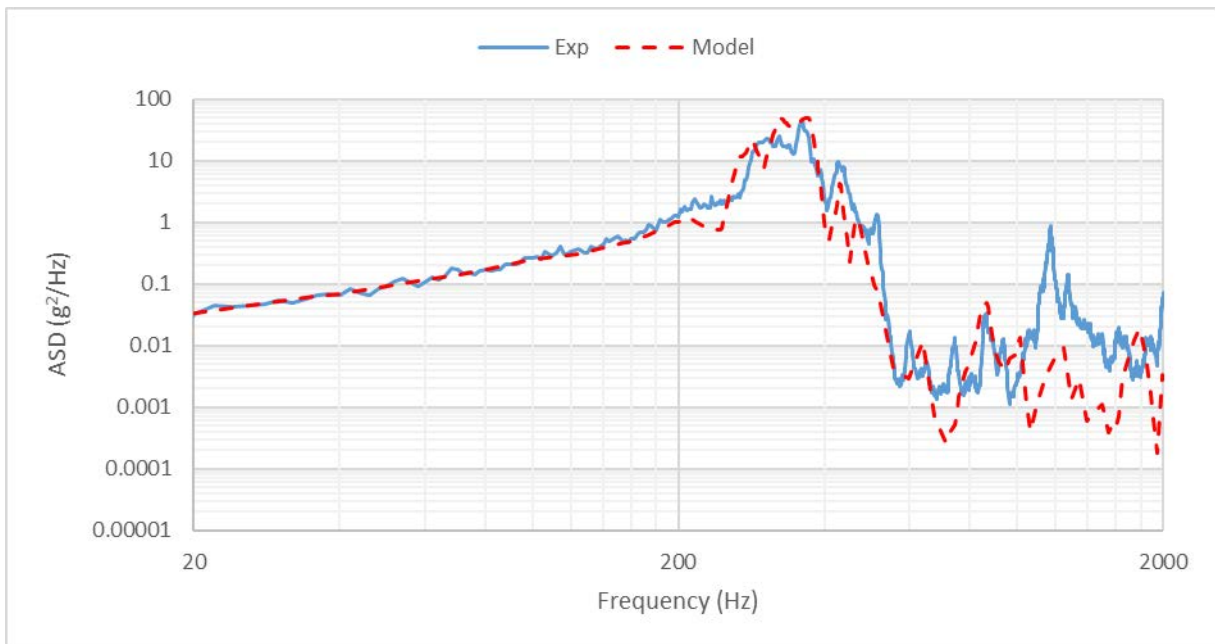


Fig.13: Z-direction ASD model comparison to random vibration test for an electronics board using frequency-dependent damping to match ASD amplitude throughout the spectrum; experimental data in solid blue; model data in dashed red.

### 4.3 Deflection Blade Fracture

As discussed in Section 3.2, a deflection blade fracture occurred during an auxiliary test procedure in which blade spacers were removed from the instrument. The failure itself was during a test that deviated from the intended flight design, and thus it did not bear judgement upon the nominal design. The failure did, however, raise a concern as to whether or not this failure could be attributed to fatigue. Visual and scanning electron microscope inspections of the fracture sites identified the points of failure initiation and observed that fractures did not appear to be fatigue-related.

The tuned model became a new tool to aid in this investigation. Eigenvalue analysis showed that the 26 blade modes that started at 118 Hz in the nominal design were lowered to frequencies between 58 and 64 Hz. This put the deflection blade natural frequencies squarely within the range of the sine sweep test at input accelerations of 13.4g. The frequency at which failure appears to have occurred is near 70 Hz. Examination of stress contours at these frequencies showed stress concentrations at the edges of the blade supports. With these observations, the FE model was able to corroborate the ductile fracture hypothesis, showing that the failure was most likely due to loading that exceeded the strength capacity of the material and not due to fatigue.

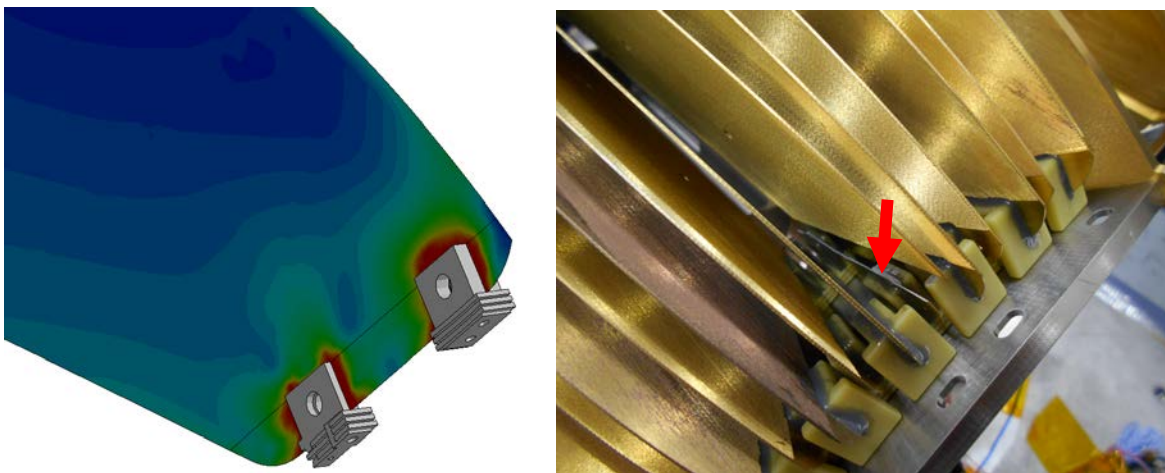


Fig.14: Left: Stress concentrations in a deflection blade near the blade supports at 61 Hz; Right: Image of the fracture edge running along the edge of the blade support

## 5 NASTRAN Comparison

While validation to experiment is itself sufficient to demonstrate the validity of the LS-DYNA results, NASTRAN is typically recognized as the industry leader and standard for normal modes and vibration analysis of spacecraft. For compatibility purposes, it is also convenient to have a NASTRAN version of the JENI model available for larger ESA analyses of the spacecraft system. While LS-PrePost, Primer [11], and other preprocessing software have some capability to convert LS-DYNA models to NASTRAN files, the converters are limited to a small subset of keywords that can be converted. In order to facilitate complete and automatic model conversion, a Python script was created to convert nearly all of the keywords used in the JENI model to NASTRAN commands [10]. Tied contacts were converted to RBE3 and RBE2 elements using a tool in the Primer Preprocessor from the Oasys suite of finite element software [11].

Results between the two solvers do not result in exact agreement, however they do show significant similarity when comparing the extracted normal modes and associated effective modal mass contributions. Most major modes show between 1% and 5% difference between the two models and the major mode shapes are the same (Fig. 15). Random vibration solutions result in good agreement between solvers in both ASD output (Fig. 16) and in RMS stress output (Fig. 17).

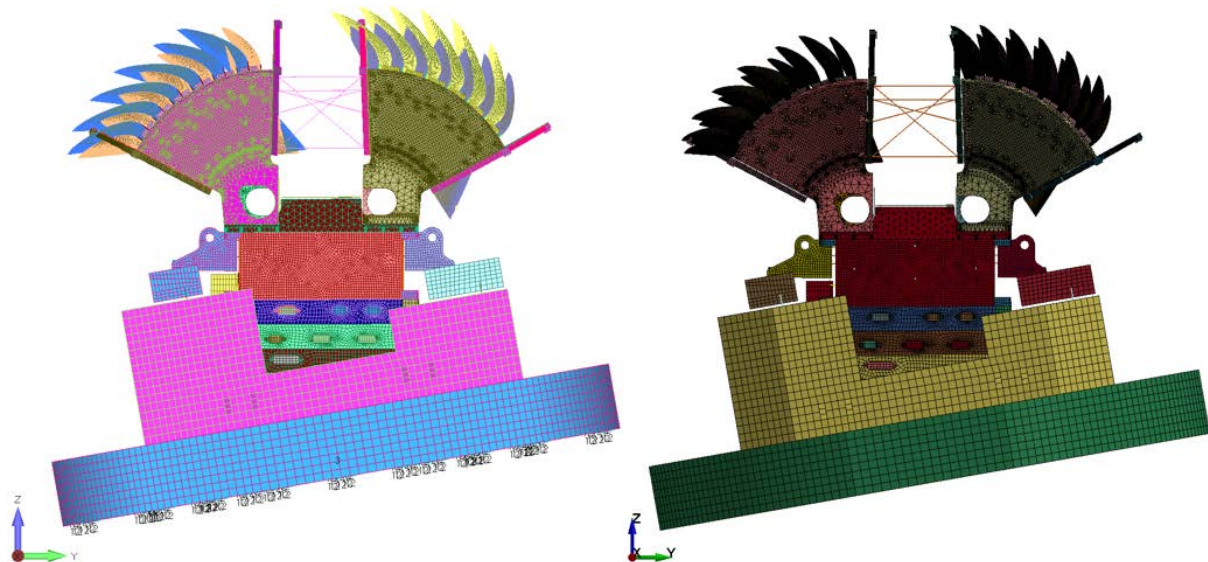


Fig. 15: First mode shape for NASTRAN model (left) at 116.7 Hz and LS-DYNA (right) at 117.6 Hz

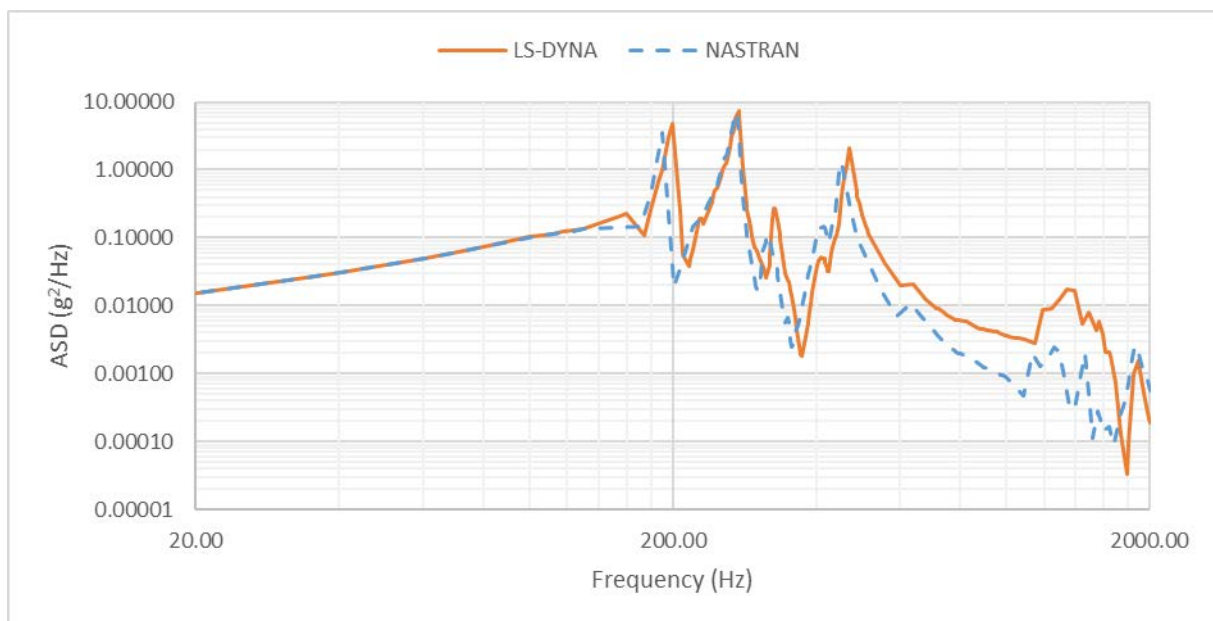


Fig. 16: X-direction ASDs at the top housing accelerometer for the LS-DYNA model (solid orange) and the NASTRAN model

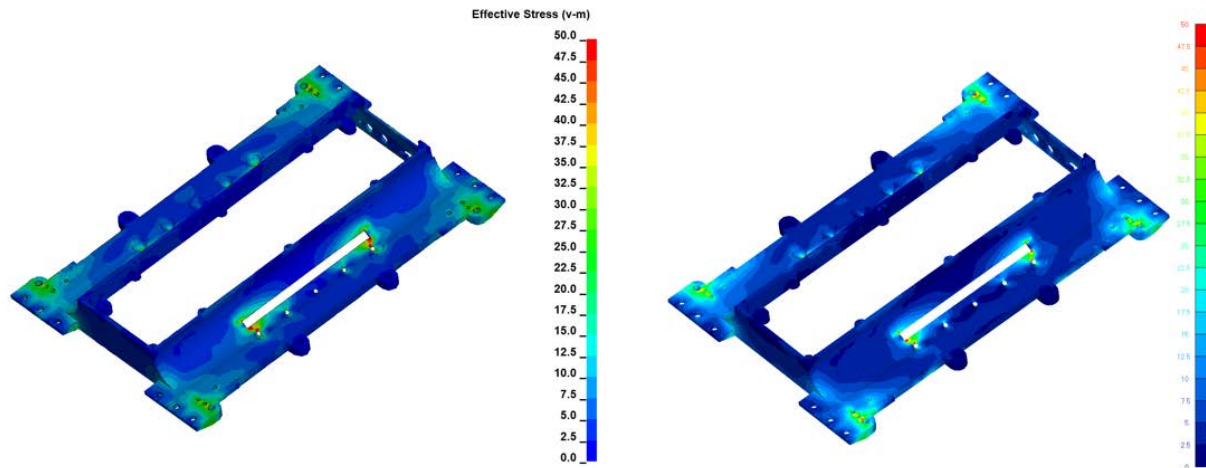


Fig.17: RMS von Mises stress contours of the tungsten-copper top housing component; the LS-DYNA model (left) is postprocessed in LS-PrePost; the NASTRAN model (right) is postprocessed in FEMAP.

## 6 Conclusions

LS-DYNA has been demonstrated as a capable tool for the purposes of qualifying the JENI space instrument for flight. Even before interface adjustments, the eigenvalue solver was able to predict major vibration mode patterns that appeared during the experimental vibration test. Optimization of the model to better represent the experimental results was simple using the eigenvalue, frequency response function, and random vibration solvers, largely due to the familiar contact algorithms and efficient MPP solvers that made changes simple and turnover time short. Even with broadband, low-level damping providing fairly conservative amplitudes, the model and experimental output line up very well when replicating sine survey and random vibration results. For reduced conservatism and more realistic amplitudes, frequency-dependent damping of the FE model has been shown to provide very close agreement with experimental results. In addition to test validation, results from LS-DYNA and a NASTRAN converted model are in agreement in regard to normal modes and random vibration analysis.

## 7 Literature

- [1] Mitchell, D.G.: "Energetic particle imaging: The evolution of techniques in imaging high-energy neutral atom emissions", Journal of Geophysical Research: Space Physics, 2016
- [2] Steinberg, D.S.: "Vibration Analysis for Electronic Equipment", 2<sup>nd</sup> Edition, 1988
- [3] LSTC: "LS-DYNA Keyword User's Manual Volume I", LS-DYNA R10.0, 2017
- [4] Huang, Y.: "Development of Frequency Domain Dynamic and Acoustic Capabilities in LS-DYNA", 8<sup>th</sup> European LS-DYNA Conference Proceedings, 2011
- [5] NASA: "NASA-HDBK-7004: Force Limited Vibration Testing", Revision C, 2012
- [6] Shor, O.: "Simulation of a Thin Walled Aluminum Tube Subjected to Base Acceleration Using LS-DYNA's Vibro-Acoustic Solver", 11<sup>th</sup> International LS-DYNA User's Conference Proceedings, 2010
- [7] Huang, Y.: "Implementation and Validation of Frequency Response Function in LS-DYNA", 2014
- [8] Jonsson, A.: "Some guidelines for implicit analyses using LS-DYNA", DYNAMore Nordic Technical Guideline, 2015
- [9] Simmons, R.: "Creating a Random Vibration Component Test Specification", NASA FEMCI The Book Website, 1997
- [10] Siemens: "NX Nastran 12 Quick Reference Guide", NX Nastran 12, 2017
- [11] Oasys Ltd.: "Primer Manual", Primer 15.0, 2018